

Accepted by **Journal of Biomechanics**

Original Article

A Mechanics Model of Microtubule Buckling in Living Cells

Teng Li*

* Corresponding author

Affiliation: Department of Mechanical Engineering and Maryland NanoCenter, University of Maryland, College Park, MD 20742, USA

Electronic mail: LiT@umd.edu

Telephone: +1 301 405 0364

Fax: +1 301 314 9477

Keywords: microtubule, buckling, cytoskeleton, mechanics modeling

Abstract

As the most rigid cytoskeletal filaments, microtubules bear compressive forces in living cells, balancing the tensile forces within the cytoskeleton to maintain the cell shape. It is often observed that, in living cells, microtubules under compression severely buckle into short wavelengths. By contrast, when compressed, isolated microtubules *in vitro* buckle into single long-wavelength arcs. The critical buckling force of the microtubules *in vitro* is two orders of magnitude lower than that of the microtubules in living cells. To explain this discrepancy, we describe a mechanics model of microtubule buckling in living cells. The model investigates the effect of the surrounding filament network and the cytosol on the microtubule buckling. The results show that, while the buckling wavelength is set by the interplay between the microtubules and the elastic surrounding filament network, the buckling growth rate is set by the viscous cytosol. By considering the nonlinear deformation of the buckled microtubule, the buckling amplitude can be determined at the kinetically constrained equilibrium. The model quantitatively correlates the microtubule bending rigidity, the surrounding filament network elasticity, and the cytosol viscosity with the buckling wavelength, the buckling growth rate, and the buckling amplitude of the microtubules. Such results shed light on designing a unified experimental protocol to measure various critical mechanical properties of subcellular structures in living cells.

1. Introduction

The mechanical properties of a cell are largely determined by its cytoskeleton (e.g., Hesketh and Prym, 1995; Howard, 2001; Boal, 2002), a self-organizing network of three primary protein filaments: microtubules, intermediate filaments, and actin filaments. Among the three types of cytoskeletal filaments, microtubules are the most rigid. The bending rigidity of microtubules is about 100 times that of intermediate and actin filaments (Gittes et al., 1993; Howard, 2001). Microtubules are hollow cylindrical tubes that are made of α - β tubulin heterodimers assembled into protofilaments (e.g., Hesketh and Prym, 1995). The rigid microtubules in living cells bear compressive forces, balancing tensile forces carried by the compliant actin and intermediate filaments — forming a synergic “skeleton” to stabilize the cell shape (Wang et al., 1993; Ingber, 1997; Maniotis et al., 1997; Stamenovic et al., 2002). Such a concept is referred to as the “tensegrity” model, first introduced by Ingber in 1997.

A microtubule buckles when subjected to a sufficiently large axial compressive force. The microtubule buckling has been observed in various types of living cells (Odde et al., 1999; Heidemann et al., 1999; Wang et al. 2001; Brangwynne et al., 2006), resulting from stimulated or spontaneous cell contraction, or constrained microtubule polymerization at the cell periphery. In some *in vitro* studies, the buckling has also been observed in microtubules encapsulated in vesicles (Elbaum et al., 1996; Fygenson et al., 1997), or in isolated microtubules under axial compressive forces generated by the kinesin motors (Gittes et al., 1996) or by the external optical tweezers (Kurachi et al., 1995; Kikumoto et al., 2006).

The microtubule buckling behaviors in living cells and *in vitro* are substantially different. Although the persistence length of microtubules (1~6 μ m) is tens of times larger than the typical size of a cell (Pampaloni et al., 2006), the microtubule buckling in living cells often occurs at

short wavelengths (e.g., several μm), suggesting that these microtubules bear large compressive forces ($\sim 100\text{s pN}$) (Wang et al., 2001; Brangwynne et al., 2006). However, *in vitro* studies suggest that isolated microtubules buckle into single long arcs (analogous to the buckling of a straw in the air when both its ends are compressed). These microtubules *in vitro* are shown to bear exceedingly small compressive forces ($\sim 1\text{ pN}$) (Volokh et al., 2000; Dogterom et al., 2005). The critical buckling force characterizes the capability of microtubules to stabilize the cell shape. The huge difference in the buckling wavelength as well as the critical buckling forces of the microtubules in living cells and those *in vitro* leaves the structural role of microtubules elusive.

There have been numerous theoretical and experimental studies on the mechanics of microtubules recently, e.g., elastic buckling (Brodland and Gordon, 1990; Kurachi et al., 1995; Elbaum et al., 1996; Coughlin and Stamenovic, 1997; Wang et al., 2001; Wang et al., 2006; Brangwynne et al., 2006), morphological instability (Janson et al., 2003; Molodtsov et al., 2005; Grishchuk et al., 2005;), and free vibration (Sirenko et al., 1996; Portet et al., 2005). While models at atomistic and molecular scales have shed important light on understanding the mechanical properties of detail microtubule nanostructure (Molodtsov et al. 2005; Tuszynski et al., 2005), continuum elastic beam models have been often used to study the deformation behavior of whole microtubules (Kurachi et al., 1995; Fygenon et al., 1997; Wang et al., 2006; Brangwynne et al., 2006). For example, Euler beam theory has been used to determine the microtubule critical buckling force. Insights from the atomistic and molecular scale studies of microtubules have also been embedded into continuum models to reflect the nanostructure-related mechanical properties, e.g., the elastic anisotropy (Tuszynski et al., 2005; Pampaloni et al., 2006). Some mechanics models on microtubule buckling consider free microtubules (e.g., Elbaum et al., 1996; Fygenon et al., 1997), without taking into account of the effect of the

surrounding cytoplasm. As a result, such a free microtubule always buckles into a single long arc and the predicted critical buckling force is exceedingly small (~ 1 pN), suggesting an insignificant structural role of microtubules in living cells. Brodland and Gordon (1990) first proposed a model of microtubule buckling constrained by the elastic intermediate filaments and showed that the reinforcing filaments prevent the long-wavelength buckling of microtubules. Their model was then extended using the post-buckling equilibrium theory to study the microtubule buckling in cultured smooth muscle cells (Stamenovic et al., 2002). This extended model predicted an average critical buckling force of microtubules of ~ 27 pN in those cells. A more recent study (Brangwynne et al., 2006) showed that the microtubules in living cells do bear large compressive forces (~ 100 pN) by buckling into short-wavelengths. It is suggested that the short-wavelength buckling results from the mechanical coupling between the microtubules and the surrounding elastic filament network. Such a model was further adopted to explain the short-wavelength buckling of microtubule bundles driven by polymerization forces (Guo et al., 2007).

In living cells, the rigid microtubules are surrounded not only by the soft *elastic* filament network, but also by the *viscous* cytosol. The microtubule buckling causes not only the elastic deformation of the filament network, but also the viscous flow of the cytosol. In turn, these two processes result in an external stress field that influences the microtubule buckling mode and kinetics. For example, the microtubule buckling at long wavelength requires viscous mass transportation of the cytosol over long distance, which is unlikely to occur incipiently. Above said, to understand the microtubule buckling behavior in living cells, it is essential to investigate the coupled effect of the elastic filament network and the viscous cytosol.

To address the abovementioned controversy in the structural role of microtubules in living cells, this paper describes a mechanics model of microtubule buckling, considering the coupled

effect of the viscoelastic surrounding cytoplasm. The model quantitatively correlates the microtubule bending rigidity, the surrounding filament network elasticity, and the cytosol viscosity with the buckling wavelength, the buckling growth rate, and the buckling amplitude of the microtubules. Such quantitative results can be potentially used to design a unified experimental protocol to measure various critical subcellular mechanical properties in living cells.

2. Mechanics model

Consider an initially straight, elastic microtubule, subject to an axial compression f_0 , in a viscoelastic surrounding of elastic modulus of E_c and viscosity of μ (the combined effect of surrounding filament network and cytosol). The microtubule is modeled as an infinitely long cylinder of radius R_0 , with a bending rigidity EI equivalent to that of the actual hollow microtubule. The incipient microtubule buckling under the compression f_0 is introduced as a sinusoidal perturbation of the center line of the microtubule, of wavelength $2\pi/k$ and amplitude $w(z,t) = w(t)\sin(kz)$ (Fig. 1a). We next determine the further growth of the incipient buckling by solving the elastic deformation of the microtubule and the surrounding filament network, as well as the resulting viscous flow of the cytosol. The elastic deformation and the viscous flow are then coupled through the interface between the microtubule and the surrounding cytoplasm, where the displacements and the tractions are assumed to be continuous.

2.1. Elastic deformation of the microtubule and the surrounding filament network

Upon incipient buckling of the microtubule, the surrounding filament network is deformed. In turn, the elastic filament network exerts a distributed surface traction on the microtubule in the opposite direction of the incipient buckling. The total resultant lateral surface traction on the microtubule can be determined by the Euler beam theory

$$F_e = -EI \frac{\partial^4 w(z,t)}{\partial z^4} - f_0 \frac{\partial^2 w(z,t)}{\partial z^2} - \zeta w(z,t), \quad (1)$$

where $\zeta \approx 2.7E_c$ (Landau and Lifshitz, 1986; Bazant and Cedolin, 1991). The three terms in Eq. (1) represent the contributions from the microtubule bending, the axial compression, and the elastic constraint from the surrounding filament network, respectively. Given that $w(z,t) = w(t)\sin(kz)$, we have

$$F_e = -(EI k^4 - f_0 k^2 + \zeta) w(t) \sin(kz). \quad (2)$$

Note that the surface traction F_e on the microtubule is linearly proportional to the incipient buckling amplitude $w(t)$.

2.2. Viscous flow of the cytosol

The incipient buckling of the microtubule also results in the viscous flow of the cytosol. The motion equation of such a viscous flow is

$$\sigma_{ij,j} = 0, \quad (3)$$

where σ_{ij} is the stress tensor of the cytosol. The inertia term is neglected in Eq. (3) since the induced cytosol flow is assumed to be slow. We assume a Newtonian deformation law of the viscous cytosol. Thus the stress components relates to the velocities by

$$\sigma_{ij} = \mu(v_{i,j} + v_{j,i}) - p\delta_{ij}, \quad (4)$$

where v_i are the velocity components, δ_{ij} is the Kronecker delta, and $p = -\frac{1}{3}\sigma_{kk}$.

The continuity equation of the incompressible viscous flow is

$$v_{i,i} = 0. \quad (5)$$

Assuming a no-slip condition at the interface between the microtubule and the cytoplasm, the velocities of the cytosol at the interface is given by

$$\begin{aligned}v_r(R_0, \theta) &= v_0 \sin(kz) \cos \theta, \\v_\theta(R_0, \theta) &= v_0 \sin(kz) \sin \theta,\end{aligned}\tag{6}$$

where v_0 is the velocity of the microtubule in the incipient buckling direction, and θ is the azimuthal angle relative to the plane in which the incipient buckling occurs (Fig. 1b). The induced viscous flow of the cytosol decays spatially away from the microtubule and vanishes at a certain distance R_1 from the center line of the microtubule (e.g., about the half spacing between adjacent microtubules), that is,

$$v_r(R_1, \theta) = v_\theta(R_1, \theta) = 0.\tag{7}$$

The above boundary value problem (i.e., Eqs. (3)-(7)) can be solved analytically to determine the stress field of the induced viscous flow in the cytosol (see Appendix for details). By integrating the stress field along the microtubule/cytoplasm interface, the surface traction of the cytosol along the interface can be given by

$$F_v = \pi\mu\chi v_0 \sin(kz),\tag{8}$$

where $\chi = \frac{(1-q^4)\ln q - 12q^2 + 2q^4 + 10}{(q^4 - 1)\ln q + 2q^2 - q^4 - 1}$ and $q = R_0 / R_1$.

Note the surface traction F_v of the cytosol is linearly proportional to the velocity of the microtubule v_0 in the incipient buckling direction.

2.3. Coupled elastic deformation and viscous flow

To couple the elastic deformation of the microtubule and the filament network with the viscous flow of the cytosol, we assume that the tractions and the displacements are continuous across the interface, that is,

$$\begin{aligned}F_e &= F_v, \\v_0 &= \frac{dw(t)}{dt}.\end{aligned}\tag{9}$$

Substituting Eqs. (2) and (8) into Eq. (9), we have

$$\frac{dw(t)}{dt} = \alpha w(t), \quad (10)$$

where

$$\alpha = -\frac{EIk^4 - f_0k^2 + \zeta}{\pi\mu\chi}. \quad (11)$$

The solution of Eq. (10) takes the form

$$w(t) = w_0 \exp(\alpha t), \quad (12)$$

where w_0 is the initial buckling amplitude. Such a solution indicates that the amplitude of the incipient microtubule buckling will grow (or decay) *exponentially* at a rate of α .

Figure 2 schematically plots the buckling growth rate α as a function of incipient buckling wave number k . Two critical wave numbers

$$k_{cr}^{\pm} = \sqrt{\frac{f_0 \pm \sqrt{f_0^2 - 4EI\zeta}}{2EI}} \quad (13)$$

can be determined at which $\alpha = 0$. If the wavelength of the incipient buckling is too long (i.e., $k < k_{cr}^-$) or too short (i.e., $k > k_{cr}^+$), $\alpha < 0$, that is, the incipient buckling of the microtubule decays, thus eventually the microtubule straightens up. For an incipient buckling at an intermediate wavelength (i.e., $k_{cr}^- < k < k_{cr}^+$), $\alpha > 0$, that is, the incipient buckling grows, leading to the microtubule buckling of large amplitude.

The above results can be explained by an energetic consideration. Buckling of the microtubule results in the increase in the contour length, thus mitigates the compressive stress in the microtubule, leading to a decrease in the microtubule elastic energy ΔU_e , thus driving the buckling to grow. On the other hand, buckling also results in an increase in the microtubule

bending energy ΔU_b , and an increase of the elastic energy of the surrounding filament network ΔU_f . For an incipient buckling at a sufficiently short wavelength (e.g., $k > k_{cr}^+$), ΔU_b outweighs ΔU_e , causing the decay of the incipient buckling. Similarly, for an incipient buckling at a sufficiently long wavelength (e.g., $k < k_{cr}^-$), ΔU_f overbalances ΔU_e , also leading to the decay of the incipient buckling. For an intermediate wavelength $k_{cr}^- < k < k_{cr}^+$, ΔU_e surpasses $\Delta U_b + \Delta U_f$, thus the incipient buckling grows exponentially.

The values of k_{cr}^\pm are real only for a compressive force that exceeds a threshold value of $f_c = 2\sqrt{EI\zeta}$, the critical Euler buckling force of the microtubule. At such a threshold compressive force, the two critical wave numbers are identical $k_{cr} = (\zeta/EI)^{1/4}$. The wave number corresponding to the fastest buckling growth rate α_{\max} is determined by $d\alpha/dk = 0$. From Eq. (11), such a fastest growing wave number is given by

$$k_{\text{fastest}} = \sqrt{\frac{f_0}{2EI}}. \quad (14)$$

The predicted microtubule buckling wave number in (Brangwynne et al., 2006) corresponds to the special case of $f_0 = f_c$.

2.4. Wavelength and growth rate of the microtubule buckling

Figures 3a and 3b plot the normalized buckling growth rate $\alpha\pi\mu\chi R_0^4/EI$ as a function of normalized buckling wave number R_0k for various axial compression f_0 and surrounding filament network elasticity E_c , respectively. For a given E_c (Fig. 3a), the buckling growth rate α and the range of possible buckling wave number ($k_{cr}^+ - k_{cr}^-$) increase as f_0 increases. The dotted curve corresponds to the case of $f_0 = f_c$. For a given f_0 (Fig. 3b), α and $k_{cr}^+ - k_{cr}^-$ increase as E_c

decreases. In the limiting case of $E_c = 0$, the incipient perturbation of any wave number $k < k_{cr}^+$ can grow, but the growth rate becomes negligible as k tends to zero. Here we use the reported microtubule bending rigidity $EI = 5 \times 10^{-24} \text{ Nm}^2$ (Felgner et al, 1996), elastic modulus $E = 2 \text{ GPa}$, $R_0 = 12.5 \text{ nm}$ (Howard, 2001).

Figure 4 plots the normalized fastest buckling growth rate $\alpha_{\max} \pi \mu \chi R_0^4 / EI$ as a function of the normalized axial compression $f_0 R_0^2 / EI$ for various surrounding filament network elasticity E_c . For a given E_c , α_{\max} increases as f_0 increases. For a given f_0 , α_{\max} increases as E_c decreases. The horizontal secant of a given curve in Fig. 4 corresponds to the threshold compression f_c .

2.5. Amplitude of the microtubule buckling at kinetically constrained equilibrium

Given the highly dynamic environment inside living cells, the buckled microtubules may not have enough time to reach their thermodynamic equilibrium. For example, a microtubule that buckles at a short wavelength can have an elastic energy higher than that at the thermodynamic equilibrium. But such a microtubule may stay at that buckled shape with certain amplitude for a long time due to the kinetic constrain of the viscous cytoplasm. We next determine the amplitude of the microtubule buckling at such a kinetically constrained equilibrium A_{eq} .

At such an equilibrium, the viscous flow of the cytosol stops, therefore the interface tractions vanish. Euler beam theory gives

$$EI \frac{d^4 w(z)}{dz^4} + f \frac{d^2 w(z)}{dz^2} + \zeta w(z) = 0. \quad (15)$$

where f is the total axial compression in the microtubule at the kinetically constrained equilibrium. By assuming $w(z) = A_{eq} \sin(kz)$, Eq. (15) gives

$$f = EI k^2 + \frac{\zeta}{k^2}. \quad (16)$$

The total axial compression f can be decomposed into two parts

$$f = f_0 + f_{extra}, \quad (17)$$

where f_{extra} is the extra compression due to the nonlinear axial strain in the microtubule under large amplitude buckling. The axial component of the nonlinear Green strain (Landau and Lifshitz, 1986; Timoshenko and Woinowsky-Krieger, 1987) is defined by

$$\varepsilon_z = \frac{\partial u_z}{\partial z} + \frac{1}{2} \left(\frac{\partial w(z)}{\partial z} \right)^2, \quad (18)$$

where u_z is the axial deformation of the microtubule. An elasticity consideration of the microtubule then gives

$$f_{extra} = \frac{ES(1-\nu)}{(1-2\nu)(1+\nu)} \left(\frac{\partial u_z}{\partial z} + \frac{1}{2} \left(\frac{\partial w(z)}{\partial z} \right)^2 \right), \quad (19)$$

where ν and S are the Poisson's ratio and the cross-section area of the microtubule, respectively. Since the tractions along the microtubule/cytoplasm interface vanish at the kinetically constrained equilibrium, the axial force f in the microtubule should be independent of z . From Eqs. (17) and (19), we have

$$u_z = -\frac{1}{8} k A_{eq}^2 \sin(2kz). \quad (20)$$

Equation (19) then becomes

$$f_{extra} = \frac{ESk^2 A_{eq}^2 (1-\nu)}{4(1-2\nu)(1+\nu)}. \quad (21)$$

Substituting Eqs. (16) and (21) into Eq. (17), we have

$$A_{eq} = \sqrt{-\frac{4(1-2\nu)(1+\nu)(EIk^2 + \xi/k^2 - f_0)}{(1-\nu)ESk^2}}. \quad (22)$$

Figures 5a and 5b plot the normalized microtubule buckling amplitude at the kinetically constrained equilibrium A_{eq}/R_0 as a function of the normalized buckling wave number R_0k for various f_0 and E_c , respectively. For a given E_c (Fig. 5a), A_{eq} increases as f_0 increases. The intersections of each curve with the horizontal axis correspond to k_{cr}^{\pm} . For a given f_0 (Fig. 5b), A_{eq} increases as E_c decreases. In the limiting case of $E_c = 0$, the buckling amplitude of the microtubule may grow without boundary. For $E_c > 0$, the maximum buckling amplitude at the kinetically constrained equilibrium occurs at a wavelength longer than that corresponding to α_{max} . Here we use the reported Poisson's ratio for macromolecules $\nu = 0.3$ (Sirenko et al., 1996).

3. Discussion

The microtubule buckling in living cells is constrained by both the elastic surrounding filament network and the viscous cytosol. While the elastic properties of the microtubule and the surrounding filament network define the critical buckling force, the viscosity of the cytosol sets how fast the buckling develops. The interplay between the buckled microtubule and the viscoelastic surrounding parallels that between a wrinkled elastic film and the underlying viscoelastic substrate (Huang and Suo, 2002; Huang, 2005). Under an axial compressive force larger than the critical buckling force, a microtubule may buckle into a wide range of wavelengths, and the buckling amplitude in any wavelength in this range can be determined at the kinetically constrained equilibrium. While the microtubule buckling may occur at a wide range of wavelengths, it is likely that the wavelength corresponding to the fastest growth rate sets the final buckled shape of the microtubule. For example, in Figure 3a, such a wavelength is predicted to be $2.6\mu\text{m}$, $2.2\mu\text{m}$ and $1.8\mu\text{m}$ for a microtubule subject to an axial compression of 232 pN, 350 pN and 500 pN, respectively. These predicted microtubule buckling wavelengths

are in good agreement with the observed buckling wavelengths ($2.8 \pm 0.6 \mu\text{m}$) of the microtubules in Cos7 epithelial cells and bovine capillary endothelial cells under exogenous compressive forces (Brangwynne et al., 2006).

Existing methods to measure subcellular mechanical properties vary for different subcellular structures. For example, the microtubule bending rigidity EI has been measured via thermal fluctuation (Gittes et al., 1993; Mickey and Howard, 1995; Janson and Dogterom, 2004), atomic force microscopy (de Pablo et al., 2003; Kis et al., 2002; Schaap et al., 2004), and optical tweezers (Kurachi et al., 1995; Felgner et al., 1996; Kikumoto et al., 2006). The viscoelastic properties of the cytoplasm can be measured by the microrheology techniques (e.g., Deng et al., 2006). The mechanical interactions among different subcellular structures are often not considered in measuring individual components. The present model quantitatively correlates critical subcellular mechanical properties, such as E_c , μ and EI with easy-to-measure microtubule buckling characteristics (e.g., α_{\max} , A_{eq} and $k_{fastest}$). Therefore, this model sheds light on designing a unified experimental protocol to measure various mechanical properties of subcellular structures. For example, Fig. 5 can be used to measure E_c if f_0 is given (e.g., by manipulating a microtubule through an optical trapping force). With E_c measured, Figs. 3 and 4 can then be used to determine μ and EI .

The mechanical properties of real microtubules are orthotropic, while the present model assumes the microtubule isotropic. A recent study showed that the isotropic elastic column model of the microtubules agrees well with the orthotropic shell model for axial buckling of very long microtubules (Wang et al., 2006). The present model assumes the linear response of the elastic surrounding filament network and the Newtonian viscosity of the cytosol. Under large amplitude microtubule buckling, the elastic constraint of the filament network may become

nonlinear with the buckling amplitude, and the velocity gradients of the cytosol flow are large near the highly buckled microtubule. Given these considerations, the microtubule buckling amplitudes at the kinetically constrained equilibrium predicted in Section 2.5 may underestimate the actual microtubule buckling amplitude. The nonuniform surrounding filament network can cause the localized microtubule bending (Brangwynne et al., 2006). These factors will also influence the microtubule buckling (e.g., resulting in larger buckling amplitudes). A three-dimensional model considering nonlinear elastic filament network and nonlinear viscous cytosol will be necessary to accurately capture the deformation characteristics of severe microtubule buckling in living cells. We will report further studies on such aspects elsewhere.

In conclusion, a mechanics model is developed to study the microtubule buckling in living cells modulated by the surrounding viscoelastic cytoplasm. The short wavelength buckling behavior predicted by the present model is in good agreement with recent experimental data. We call for further experiments based on this quantitative model to explore a unified protocol to measure various subcellular mechanical properties in living cells.

The author acknowledges the support of a Nano-Biotechnology Initiative Award from Maryland Department of Business and Economic Development. The author also thanks the anonymous reviewers for their valuable comments on the manuscript.

Conflict of interest statement

The author states that he has no any financial, professional and personal conflict of interests.

Appendix

The incipient viscous flow of the cytosol can be assumed to be in the plane strain deformation state in the r - θ plane (Fig. 1b). The 2-D motion equations in the r - θ plane reduce to

$$\frac{\partial p}{\partial r} = \mu \left(\nabla^2 v_r - \frac{v_r}{r^2} - \frac{2}{r^2} \frac{\partial v_r}{\partial \theta} \right) \quad (23)$$

$$\frac{1}{r} \frac{\partial p}{\partial \theta} = \mu \left(\nabla^2 v_\theta - \frac{v_\theta}{r^2} + \frac{2}{r^2} \frac{\partial v_r}{\partial \theta} \right) \quad (24)$$

whereas the continuity equation takes the form

$$\frac{\partial v_r}{\partial r} + \frac{v_r}{r} + \frac{1}{r} \frac{\partial v_\theta}{\partial \theta} = 0 \quad (25)$$

By introducing a stream function ψ , that is,

$$v_r = \frac{1}{r} \frac{\partial \psi}{\partial \theta}, \quad v_\theta = -\frac{1}{r} \frac{\partial \psi}{\partial r}, \quad (26)$$

Eqs. (23) and (24) lead to

$$\nabla^4 \psi = 0, \quad (27)$$

or

$$\left(\frac{\partial^2}{\partial r^2} + \frac{1}{r} \frac{\partial}{\partial r} + \frac{1}{r^2} \frac{\partial^2}{\partial \theta^2} \right) \left(\frac{\partial^2 \psi}{\partial r^2} + \frac{1}{r} \frac{\partial \psi}{\partial r} + \frac{1}{r^2} \frac{\partial^2 \psi}{\partial \theta^2} \right) = 0. \quad (28)$$

Assuming the stream function in the form $\psi = g(r) \sin \theta \sin(kz)$, Eq. (28) reduces to

$$\left(\frac{\partial^2}{\partial r^2} + \frac{1}{r} \frac{\partial}{\partial r} - \frac{1}{r^2} \right) \left(\frac{\partial^2 g(r)}{\partial r^2} + \frac{1}{r} \frac{\partial g(r)}{\partial r} - \frac{g(r)}{r^2} \right) = 0, \quad (29)$$

whose solution takes the form

$$g(r) = Ar^3 + Br + C \frac{1}{r} + Dr \ln r, \quad (30)$$

where A, B, C and D are coefficients to be determined.

Substituting Eq. (30) into Eq. (26), we have

$$v_r = -(Ar^2 + B + C \frac{1}{r^2} + D \ln r) \cos \theta \sin(kz), \quad (31)$$

$$v_\theta = -(3Ar^2 + B - C \frac{1}{r^2} + D \ln r + D) \sin \theta \sin(kz). \quad (32)$$

By substituting Eqs. (31) and (32) into the boundary conditions (i.e., Eqs. (6) and (7)), the coefficients A, B, C and D can be solved as

$$A = \frac{-v_0 q^2 \ln q}{(1-q^2)(1-q^2+(1+q^2)\ln q)}, \quad (33)$$

$$B = \frac{v_0 R_0^2 (2 \ln q + (1-q^2)(2 \ln R_1 + 1))}{(1-q^2)(1-q^2+(1+q^2)\ln q)}, \quad (34)$$

$$C = \frac{v_0 R_0^2 R_1^2 (q^2 - 1 - \ln q)}{q^2 (1-q^2)(1-q^2+(1+q^2)\ln q)}, \quad (35)$$

$$D = \frac{-v_0 q^2}{(1-q^2)(1-q^2+(1+q^2)\ln q)}, \quad (36)$$

where $q = R_0 / R_1$.

The stress components of the cytosol at the microtubule/cytoplasm interface can be then obtained by substituting Eqs. (31)-(36) into Eq. (4),

$$\sigma_{rr} = -4\mu v_0 \cos \theta \sin(kz) \frac{(4q^4 - 2) \ln q + 3q^2 - q - 2}{R_0((q^4 - 1) \ln q - q^4 + 2q^2 - 1)} \quad (37)$$

$$\sigma_{r\theta} = 2\mu v_0 \sin \theta \sin(kz) \frac{-(3q^4 + 1) \ln q + q^4 - 1}{R_0((q^4 - 1) \ln q - q^4 + 2q^2 - 1)} \quad (38)$$

The surface traction of the cytosol along the interface can be obtained by integrating the stress field,

$$\begin{aligned} F_v &= \int_0^{2\pi} (\sigma_{rr} \cos \theta - \sigma_{r\theta} \sin \theta) R_0 d\theta \\ &= \mu v_0 \pi \sin(kz) \frac{(1-q^4) \ln q - 12q^2 + 2q^4 + 10}{(q^4 - 1) \ln q + 2q^2 - q^4 - 1} \end{aligned} \quad (39)$$

References

- Bazant, Z.P., Cedolin, L., 1991. *Stability of Structures: Elastic, Inelastic, Fracture, and Damage Theories*, Oxford University Press, New York.
- Boal, D., 2002. *Mechanics of the Cell*, Cambridge University Press, New York.
- Brangwynne, C.P., MacKintosh, F.C., Kumar, S., Geisse, N.A., Talbot, J., Mahadevan, L., Parker, K.K., Ingber, D.E., Weitz, D.A., 2006. Microtubules can bear enhanced compressive loads in living cells because of lateral reinforcement. *The Journal of Cell Biology* 173, 733-741.
- Brodland, G.W., Gordon, R., 1990. Intermediate filaments may prevent buckling of compressively loaded microtubules. *Journal of Biomechanics Engineering* 112, 319–321.
- Coughlin, M.F., Stamenovic, D., 1997. A tensegrity structure with buckling compression elements: Application to cell mechanics. *Journal of Applied Mechanics-Transactions of The ASME* 64, 480-486.
- de Pablo, P. J., Schaap, I. A. T., MacKintosh, C., Schmidt, C. F., 2003. Deformation and collapse of microtubules on the nanometer scale. *Physical Review Letters* 91, 098101.
- Deng, L., Treppe, X., Butler, J. P., Millet, E., Morgan, K.G., Weitz, D.A., Fredberg, J.J., 2006. Fast and slow dynamics of the cytoskeleton. *Nature Materials* 5, 636-640.
- Dogterom, M., Kerssemakers, J.W.J., Romet-Lemonne, G., Janson, M.E., 2005. Force generation by dynamic microtubules. *Current Opinion in Cell Biology* 17, 67–74.
- Elbaum, M., Fygenson, D.K., Libchaber, A., Buckling microtubules in vesicles, *Physical Review Letters* 76, 4078-4081.
- Felgner, H., Frank, R. and Schliwa, M., 1996. Flexural rigidity of microtubules measured with the use of optical tweezers. *Journal of Cell Science* 109, 509–516.

- Fygenson, D.K., Marko, J.F., Libchaber, A., 1997. Mechanics of Microtubule-Based Membrane Extension, *Physical Review Letters* 79, 4497-4500.
- Gittes, F., Mickey, B., Nettleton, J., Howard, J., 1993. Flexural rigidity of microtubules and actin filaments measured from thermal fluctuations in shape. *Journal of Cell Biology* 120, 923–934.
- Gittes, F., Meyhofer, E., Baek, S., Howard, J., 1996. Directional loading of the kinesin motor molecule as it buckles a microtubule. *Biophys. Journal* 70, 418–429.
- Grishchuk, E.L., Molodtsov, M.I., Ataulakhanov, F.I., McIntosh, J.R., 2005. Force production by disassembling microtubules. *Nature* 438, 384-388.
- Guo, Y., Liu, Y., Tang, J.X., Valles, J. M. Jr., 2007. Polymerization force driven buckling of microtubule bundles determines the wavelength of patterns formed in tubulin solutions, *Physical Review Letters* 98, 198103.
- Heidemann, S.R., Kaech, S., Buxbaum, R.E., Matus, A., 1999. Direct observations of the mechanical behaviors of the cytoskeleton in living fibroblasts. *Journal of Cell Biology* 145, 109–122.
- Hesketh, J.E., Prym, I.F. (Eds.), 1995. *The Cytoskeleton*. JAI Press, Greenwich.
- Howard, J., 2001. *Mechanics of Motor Proteins and the Cytoskeleton*, Sinauer Associates, Inc., Sunderland.
- Huang, R., Kinetic wrinkling of an elastic film on a viscoelastic substrate. *Journal of the Mechanics and Physics of Solids* 53, 63-89.
- Huang, R., Suo, Z., 2002. Wrinkling of a compressed elastic film on a viscous layer. *Journal of Applied Physics* 91, 1135-1142.
- Ingber, D.E., 1997. Tensegrity: the architectural basis of cellular mechanotransduction. *Annual Review of Physiology* 59, 575-599.

- Janson, M. E., Dood, M. E., Dogterom, M., 2003. Dynamic instability of microtubules is regulated by force, *Journal of Cell Biology* 161, 1029-1034.
- Janson, M.E., Dogterom, M., 2004. A bending mode analysis for growing microtubules: Evidence for a velocity-dependent rigidity. *Biophysical Journal* 87, 2723-2736.
- Kikumoto, M., Kurachi, M., Tosa, V., Tashiro, H., 2006. Flexural rigidity of individual microtubules measured by a buckling force with optical traps. *Biophysical Journal* 90, 1687-1696.
- Kis, A., Kasas, S., Babič, B., Kulik, A. J., Benoît, W., Briggs, G. A. D., Schönenberger, C., Catsicas, S., Forrò, L., 2002. Nanomechanics of microtubules. *Physical Review Letters* 89, 248101.
- Kurachi, M., Hoshi, M., Tashiro, H., 1995. Buckling of a single microtubule by optical trapping forces - direct measurement of microtubule rigidity. *Cell Motility and the Cytoskeleton* 30, 221-228.
- Landau, L.D., Lifshitz, E.M., 1986. *Theory of Elasticity*. Pergamon Press, Oxford.
- Maniotis, A.J., Chen, C.S., Ingber, D.E., 1997. Demonstration of mechanical connections between integrins cytoskeletal filaments, and nucleoplasm that stabilize nuclear structure. *Proceedings of the National Academy of Sciences of the United States of America* 94, 849-854.
- Mickey, B., Howard, J., 1995. Rigidity of microtubules is increased by stabilizing agents. *Journal of Cell Biology* 130, 909-917.
- Molodtsov, M. I., Ermakova, E. A., Shnol, E. E., Grishchuk, E. L., McIntosh, J. R., Ataulakhanov, F. I., 2005. A Molecular-Mechanical Model of the Microtubule, *Biophysical Journal* 88, 3167-3179.

- Odde, D.J., Ma, L., Briggs, A.H., DeMarco, A., Kirschner, M.W., 1999. Microtubule bending and breaking in living fibroblast cells. *Journal of Cell Science* 112, 3283-3288.
- Pampaloni, F., Lattanzi, G., Jonas, A., Surrey, T., Frey, E., Florin, E.L., 2006. Thermal fluctuations of grafted microtubules provide evidence of a length-dependent persistence length. *Proceedings of the National Academy of Sciences of the United States of America* 103, 10248-10253.
- Portet, S, Tuszyński, J. A., Hogue, C. W. V., Dixon, J. M., 2005. Elastic vibrations in seamless microtubules, *European Biophysics Journal* 34, 912-920.
- Schaap, I. A. T., de Pablo, P. J., Schmidt, C. F., 2004. Resolving the molecular structure of microtubules under physiological conditions with scanning force microscopy, *European Biophysics Journal* 33, 462–467.
- Sirenko, Y. M., Strosio, M. A., Kim, K. W., 1996. Elastic vibrations of microtubules in a fluid. *Physical Review E* 53, 1003-1010.
- Stamenovic, D., Mijailovich, S.M., Tolic-Norrelykke, I.M., Chen, J., Wang, N., 2002. Cell prestress. II. Contribution of microtubules. *The American Journal of Physiology - Cell Physiology* 282, C617–C624.
- S. Timoshenko and S. Woinowsky-Krieger, *Theory of Plates and Shells*, 1987. (2nd ed.) McGraw-Hill, New York.
- Tuszynski, J.A., Luchko, T., Portet, S. and Dixon, J.M., Anisotropic elastic properties of microtubules, *The European Physical Journal E - Soft Matter* 17, 29-35.
- Volokh, K.Y., Vilnay, O., Belsky, M., 2000. Tensegrity architecture explains linear stiffening and predicts softening of living cells. *Journal of Biomechanics* 33, 1543–1549.
- Wang, C.Y., Ru, C.Q., Mioduchowski, A., 2006. Orthotropic elastic shell model for buckling of

microtubules. *Physical Review E* 74, 052901.

Wang, N., Butler, J.P., Ingber, D.E., 1993. Mechanotransduction across the cell surface and through the cytoskeleton. *Science* 260, 1124–1127.

Wang, N., Naruse, K., Stamenovic, D., Fredberg, J.J., Mijailovich, S.M., Tolic-Norrelykke, I.M., Polte, T., Mannix, R., Ingber, D.E., 2001. Mechanical behavior in living cells consistent with the tensegrity model. *Proceedings of the National Academy of Sciences of the United States of America* 98, 7765–7770.

Figure Captions

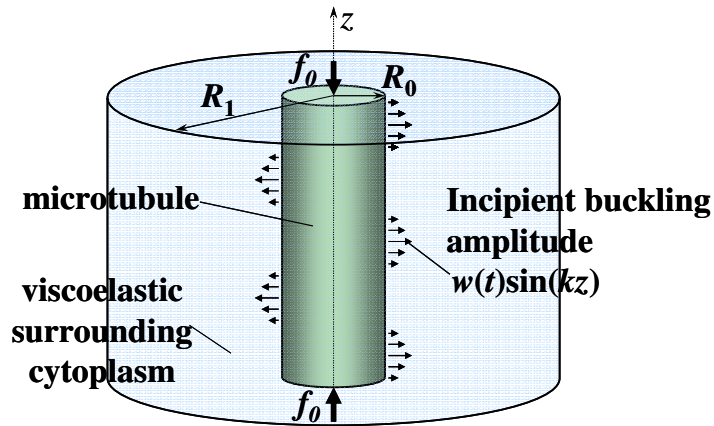
Fig. 1. (a) Schematic of an initially straight microtubule in the viscoelastic surrounding cytoplasm. Under an axial compression f_0 , the microtubule incipiently buckles into a sinusoidal shape of amplitude $w(t)\sin(kz)$. (b) The cross-section view of the microtubule in the cytoplasm. The solid and dotted circles at the center represent the microtubule's original position and its position at the incipient buckling, respectively. v_0 is the velocity of the microtubule in the incipient buckling direction. v_r and v_θ are the velocity components of the buckling-induced viscous flow of the cytosol.

Fig. 2. Schematic of the growth rate of the microtubule incipient buckling amplitude α as a function of the buckling wave number k . The microtubule buckling may occur at a range of wave number $k_{cr}^- < k < k_{cr}^+$, from which the wave number $k_{fastest}$ corresponding to the fastest growth rate α_{max} can be determined.

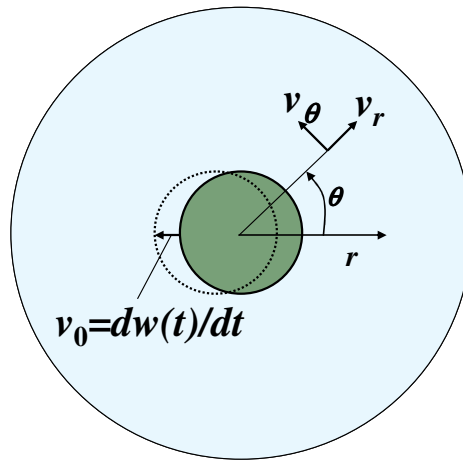
Fig. 3. The normalized buckling growth rate as a function of the normalized buckling wave number for various (a) axial compression f_0 and (b) filament network elastic modulus E_c . Here $EI = 5 \times 10^{-24} \text{ Nm}^2$, $E = 2 \text{ GPa}$, $R_0 = 12.5 \text{ nm}$.

Fig. 4. The normalized fastest buckling growth rate as a function of the normalized axial compression in the microtubule for various filament network elastic modulus E_c . Here $EI = 5 \times 10^{-24} \text{ Nm}^2$, $E = 2 \text{ GPa}$, $R_0 = 12.5 \text{ nm}$.

Fig. 5. The normalized buckling amplitude at the kinetically constrained equilibrium as a function of the normalized buckling wave number for various (a) axial compression f_0 and (b) filament network elastic modulus E_c . Here $EI = 5 \times 10^{-24} \text{ Nm}^2$, $E = 2 \text{ GPa}$, $R_0 = 12.5 \text{ nm}$.



(a)



(b)

Fig. 1. (a) Schematic of an initially straight microtubule in the viscoelastic surrounding cytoplasm. Under an axial compression f_0 , the microtubule incipiently buckles into a sinusoidal shape of amplitude $w(t)\sin(kz)$. (b) The cross-section view of the microtubule in the cytoplasm. The solid and dotted circles at the center represent the microtubule's original position and its position at the incipient buckling, respectively. v_0 is the velocity of the microtubule in the incipient buckling direction. v_r and v_θ are the velocity components of the buckling-induced viscous flow of the cytosol.

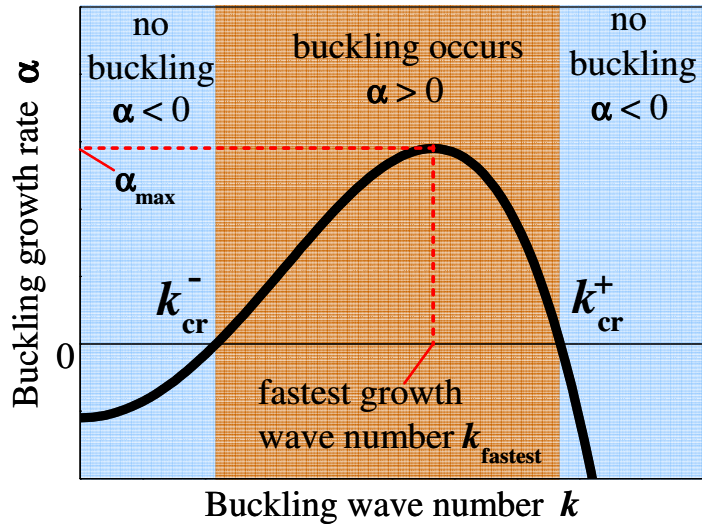
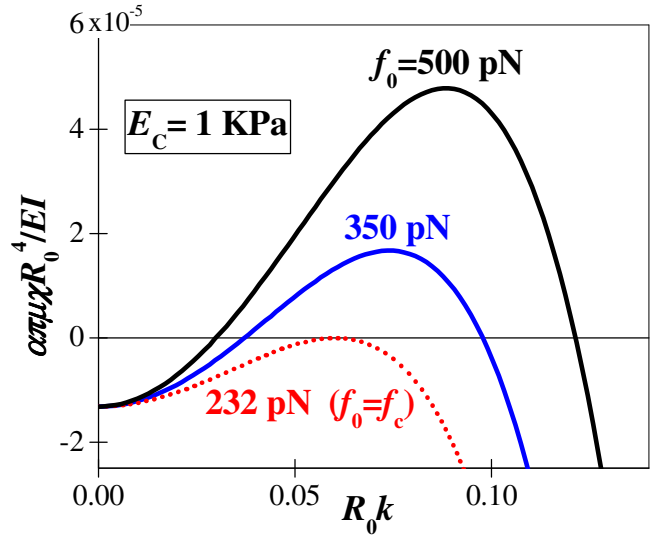
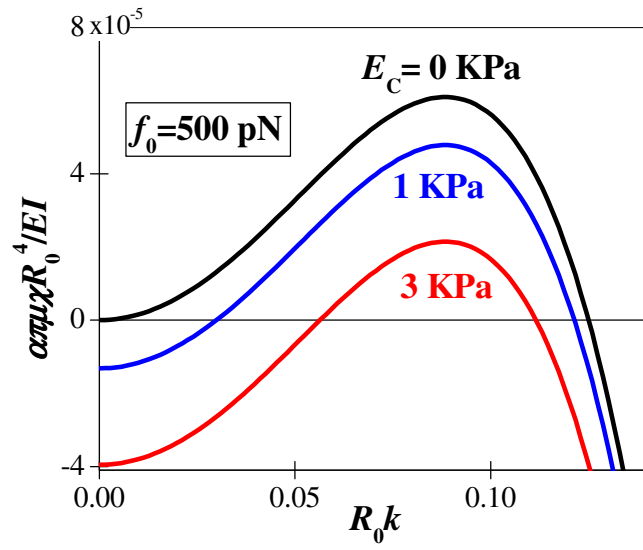


Fig. 2. Schematic of the growth rate of the microtubule incipient buckling amplitude α as a function of the buckling wave number k . The microtubule buckling may occur at a range of wave number $k_{cr}^- < k < k_{cr}^+$, from which the wave number $k_{fastest}$ corresponding to the fastest growth rate α_{max} can be determined.



(a)



(b)

Fig. 3. The normalized buckling growth rate as a function of the normalized buckling wave number for various (a) axial compression f_0 and (b) filament network elastic modulus E_c .

Here $EI = 5 \times 10^{-24} \text{ Nm}^2$, $E = 2 \text{ GPa}$, $R_0 = 12.5 \text{ nm}$.

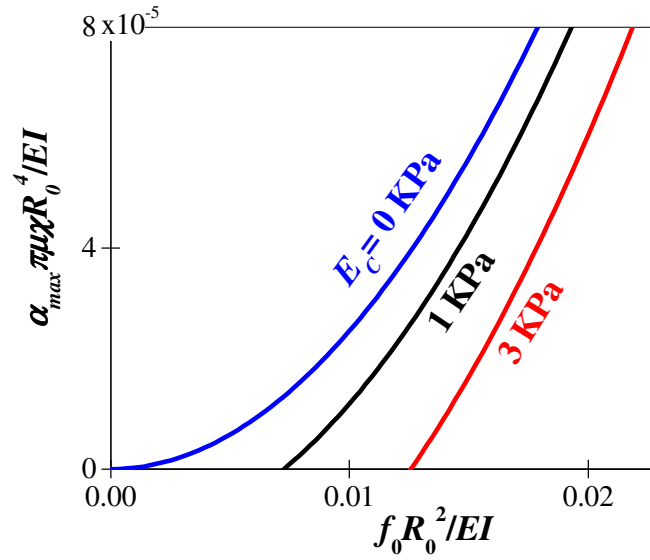


Fig. 4. The normalized fastest buckling growth rate as a function of the normalized axial compression in the microtubule for various filament network elastic modulus E_c . Here $EI = 5 \times 10^{-24} \text{ Nm}^2$, $E = 2 \text{ GPa}$, $R_0 = 12.5 \text{ nm}$.

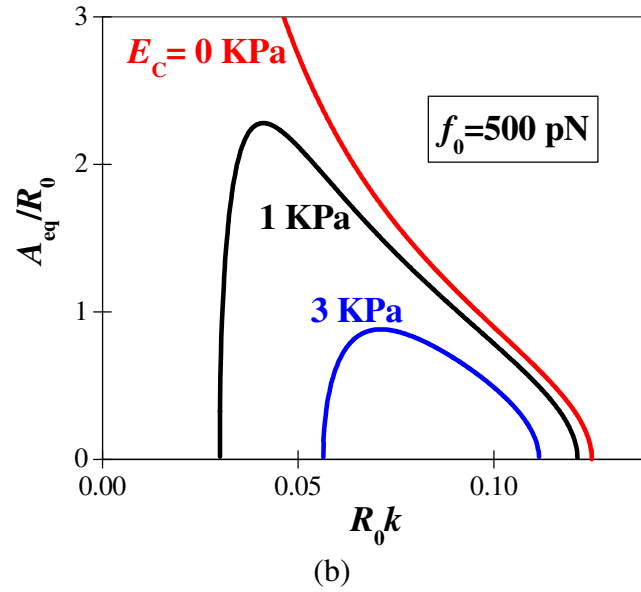
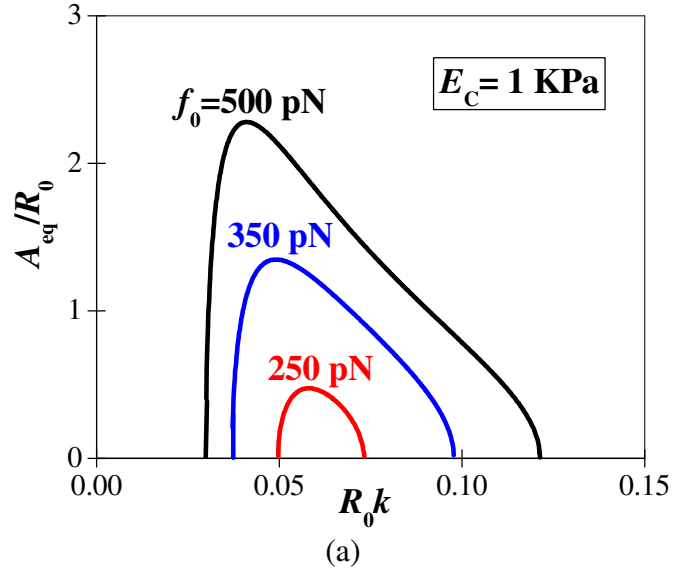


Fig. 5. The normalized buckling amplitude at the kinetically constrained equilibrium as a function of the normalized buckling wave number for various (a) axial compression f_0 and (b) filament network elastic modulus E_c . Here $EI = 5 \times 10^{-24} \text{ Nm}^2$, $E = 2 \text{ GPa}$, $R_0 = 12.5 \text{ nm}$.